Scripta Materialia 113 (2016) 23–26

Contents lists available at ScienceDirect

Scripta Materialia

journal homepage: www.elsevier.com/locate/smm

Regular Article

Influence of grain boundaries on the figure of merit of undoped and Al, In, Sn doped ZnO thin films for photovoltaic applications

A. Yildiz [a,*], S. Uzun [b], N. Serin [c], T. Serin [c]

[a] Department of Energy Systems Engineering, Faculty of Engineering and Natural Sciences, Yıldırım Beyazıt University, Ankara, Turkey
[b] Department of Engineering Physics, Faculty of Engineering, Gaziantep University, Gaziantep, Turkey
[c] Department of Engineering Physics, Faculty of Engineering, Ankara University, Ankara, Turkey

ARTICLE INFO

Article history:
Received 27 August 2015
Accepted 2 October 2015
Available online xxxx

Keywords:
ZnO
Sol–gel dip coating technique
Grain boundaries
The figure of merit
Photovoltaic applications

ABSTRACT

Electron transport in ZnO doped with 3 at.% Sn, In, and Al processed using the sol–gel dip coating technique was investigated to obtain the correlation between the type of dopant and its effect on electrical and optical properties. A detailed analysis in terms of grain boundary transport was used to correlate the values of the figure of merit with the mean potential barrier height. We found that Al dopant leads to form the lowest mean barrier height among other dopants, which remarkably improves the figure of merit.

ZnO, a *n*-type semiconductor with band gap energy of 3.37 eV, is a promising material for transparent conducting oxide applications. Its conductivity can be increased by increasing the concentration of doping ions such as Sn, In, and Al. This results from the replacing Zn^{2+} of atoms of such elements having higher valance electrons [1–6]. ZnO is not stable with the intrinsic donors due to the native defects. This situation can be overcome by adding these extrinsic atoms to its lattice [1–6]. On the other hand, once dopant concentration becomes higher than 2%, poor crystallinity and deterioration on the properties of ZnO were reported [1–3]. This behavior is due to the formation of stresses by the difference in ion size between Zn and the dopants [1–3], which results in local disorders in the lattice. At high doping level (>2%), the segregation of dopants in the grain boundaries (GBs) is also considered to be responsible of this deterioration [1–3]. At high doping level, therefore, electron transport should be related with disorders located at the GBs in ZnO.

Due to the widespread applications of ZnO, there is a considerable interest in understanding its electrical and optical properties [6–9], which is critical for further improvement of device characteristics. The GBs which significantly have an influence on the electrical and optical properties of materials are often undesired in especially electronic and optoelectronic applications. Therefore, a detailed knowledge of the electron transport mechanisms through the GBs in materials has significant implications for many improved applications. However, the influence of the GBs on the properties of ZnO is still unsatisfactory, limiting to optimize ZnO-based applications such as photovoltaic (PV) devices. Note that the efficiency of these devices is determined with the figure of merit $FM = (\sigma/\alpha)$, where σ is electrical conductivity and α is the absorption coefficient [7]. Therefore, high conductive but low absorber materials are needed to improve *FM*.

In this study, we reported on an experimental study which we expect to be helpful in achieving a more complete understanding of the GBs effect on electrical and optical properties of undoped ZnO and 3 at.% Sn-doped ZnO (hereafter TZO), 3 at.% In-doped ZnO (hereafter IZO), and 3 at.% Al-doped ZnO (hereafter AZO) processed using the sol–gel dip coating technique.

The films were coated by the sol–gel dip coating technique on ultrasonically cleaned glass substrates. The coating solution for undoped ZnO thin film was prepared by dissolving zinc acetate-2-hydrate [$Zn(CH_3COO)_2 \cdot 2H_2O$] (0.6 M) in ethanol. Thereafter, lactic acid was added to the solution and it was mixed in a magnetic stirrer. When it turned milky, diethanolamine ($HN(CH_2CH_2OH)_2$ was added as a sol stabilizer drop by drop into the solution until it became transparent. The solution was allowed to age for 24 h at room temperature before the deposition on the glass substrate. Film deposition was carried out at a controlled speed of approximately 0.5 cm/s. After coating, the substrates were baked at 500 °C for 10 min in air atmosphere. In order to increase the thickness of the film the processes were repeated 5 times. Consecutively, under similar experimental conditions, doped ZnO thin films have been elaborated by adding $InCl_3$, $SnCl_2$ and $AlCl_3$ as sources of In, Sn and Al respectively. The molar ratios In/Zn, Sn/Zn and Al/Zn were 3% wt.

The microstructure of the deposited films was investigated by means of a Rigaku Miniflex II diffractometer. The radiation source, the

* Corresponding author.
E-mail address: yildizab@gmail.com (A. Yildiz).

http://dx.doi.org/10.1016/j.scriptamat.2015.10.004
1359-6462/

wavelength and the scanning range 2θ of the diffractometer were CuKα, 0.154 nm and 25–70° respectively. The optical band gap of the films was calculated by means of UV–Vis–NIR transmittance measurements performed with Shimadzu UV-3600 spectrophotometer in the spectral range 300–1000 nm. The electrical resistance measurements were performed, as a function of temperature, with Keithley 2420 programmable constant current source in a temperature range 120–300 K.

The XRD pattern of the samples is shown in Fig. 1. All the XRD patterns show well defined peaks and the peaks of ZnO are indexed in the figure [7]. All the samples contain the hexagonal wurtzite phase of ZnO with preferred orientation along (002) plane. The (002) diffraction peak intensity varies with dopant. The highest (002) diffraction peak belongs to undoped sample. The grain size (D) of the samples was calculated by assuming grains as spherical particles ($D = \frac{0.9\lambda}{\beta\cos\theta}$, where λ is the X-ray wavelength, θ is the Bragg angle, and β is the full-width-half-maximum (FWHM) of the (002) peak) [10–12]. Estimated value of D for each sample is given in Table 1. A decrease in the grain size is observed with dopants.

Fig. 2a illustrates the transmittance spectra of the samples. The average optical transmittance value was ~84%, 74%, 76%, and 78% in the range 400–800 nm for ZnO, TZO, IZO and AZO, respectively. It also decreases with dopants. It is slightly increased with Al, the AZO sample still exhibits high transparency (~78%). The band gap energy (E_g) can be obtained using the Tauc equation ($(\alpha h\nu)^2 = A(h_\nu - E_g)$), where A is the band edge constant, and $h\nu$ is the photon energy. The band gap energies were obtained from extrapolation of the straight line portions to $\alpha h\nu = 0$ in the plot of $(\alpha h\nu)^2$ versus photon energy. Fig. 2b presents $(\alpha h\nu)^2$ versus photon energy plots. The E_g obtained from the plots slightly changes with dopants. The decrease in E_g with Sn and In dopants can be understood by formation of localized states which reduce the band gap. On the other hand, E_g widens by Al dopant due to probably its significantly high carrier concentration.

Fig. 3 displays the conductivity–temperature characteristics of the samples. The data reveal a small change of the slopes with decreasing temperature. Sn, In, and Al dopants behave as effective donors in ZnO. Since introduction of dopants increase free electron density by substituting the host Zn atom [1–6], it leads to an increase in electrical conductivity of ZnO, as seen from Fig. 3. The highest conductivity belongs to the AZO sample. This behavior can qualitatively be explained by taking into account the effect of the GBs, as explained below. We should also note that the magnitude of conductivity of the samples is found to be consistent with the previous report [1].

As seen from Fig. 3, temperature-dependent conductivity of the samples exhibits the deviations from the straight line in Arrhenius behavior [7]. Over the whole measurement range, temperature-dependent conductivity does not show an Arrhenius behavior, which indicates that the simple thermal activation behavior should be ruled out as being the dominant conduction mechanism for all samples [7]. On the other hand, it is clear from Fig. 3 that the conductivity is well described by parabola agreement, consistent with Eq. (5), as discussed below. These experimental results are consistent with the behavior of inhomogeneous GBs [13]. Various structural disorders in the GBs lead rise to potential fluctuations [13] and therefore the electron transport is limited by the potential barriers across the GBs.

Inhomogeneous at the GBs results in potential fluctuations, because of random spatial distribution of the traps, among boundaries. Electrons are captured in that interface states which locate with energy above the Fermi level. They represent a repulsive potential for free electrons crossing the interface. These electrons located at the interface leads to alter the Fermi level around the GB, which qualitatively corresponds to a band bending as a consequence [13]. The model assumes that the electrical current density (J) of majority carrier flowing across the GBs is described as [13]

$$J = A^* T^2 \exp(-q\xi/k_B T)\exp(-qV_{gb}/k_B T)[1-\exp(-qV_d/k_B T)] \quad (1)$$

Table 1
Physical parameters deduced from the plots of Figs. 1, 2b, and 3.

Sample	D (nm)	E_g (eV)	σ_{RT} $(\Omega\ \mathrm{cm})^{-1}$	$\overline{\phi}$ (meV)	σ_ϕ (meV)
ZnO	31.63	3.27	0.0006	176	48
TZO	19.72	3.25	0.0529	74	32
IZO	17.13	3.26	0.0902	61	29
AZO	12.57	3.29	0.1727	18	17

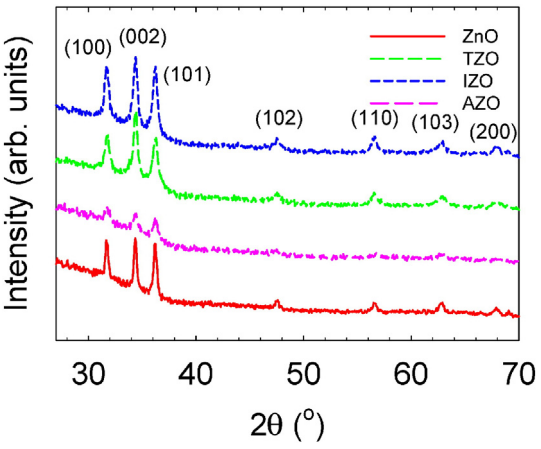

Fig. 1. X-ray diffraction patterns of the films.

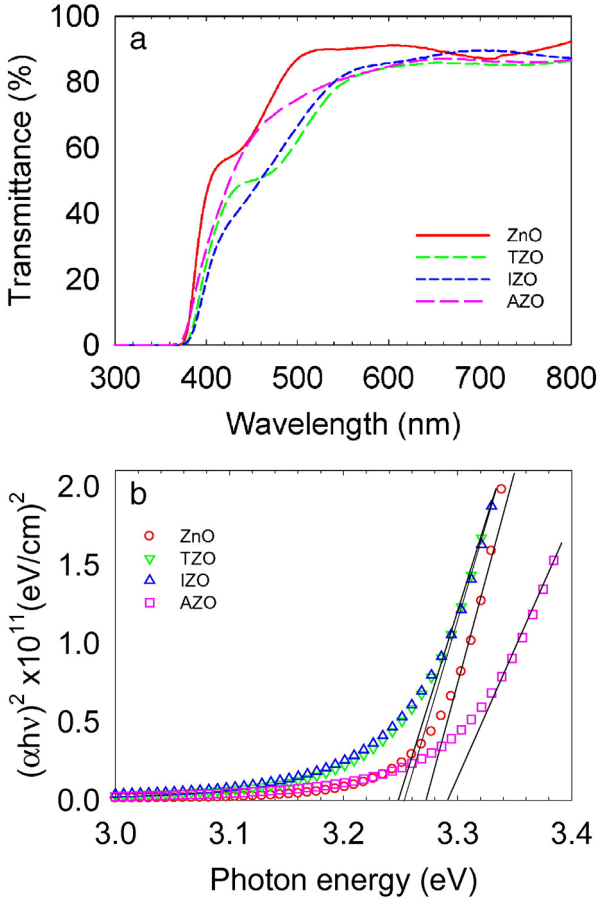

Fig. 2. (a) The optical transmittance spectra of the films, (b) plot of $(\alpha h\nu)^2$ as a function of photon energy $h\nu$ for the films.